npj | parkinson's disease

Article

Published in partnership with the Parkinson's Foundation

https://doi.org/10.1038/s41531-024-00788-x

GPR37 processing in neurodegeneration: a potential marker for Parkinson's Disease progression rate

Check for updates

Josep Argerich[1,2], Leonardo D. Garma[3], Marc López-Cano[1,2], Paula Álvarez-Montoya[1,2], Laura Gómez-Acero[1,2], Víctor Fernández-Dueñas[1,2], Ana B. Muñoz-Manchado[4,5], Ester Aso[1,2], Adam Boxer[6], Pol Andres-Benito[7], Per Svenningsson[8,9] ✉ & Francisco Ciruela[1,2] ✉

The orphan G protein-coupled receptor 37 (GPR37), widely associated with Parkinson's disease (PD), undergoes proteolytic processing under physiological conditions. The N-terminus domain is proteolyzed by a disintegrin and metalloproteinase 10 (ADAM-10), which generates various membrane receptor forms and ectodomain shedding (ecto-GPR37) in the extracellular environment. We investigated the processing and density of GPR37 in several neurodegenerative conditions, including Lewy body disease (LBD), multiple system atrophy (MSA), corticobasal degeneration (CBD), progressive supranuclear palsy (PSP), and Alzheimer's disease (AD). The presence of ecto-GPR37 peptides in the cerebrospinal fluid (CSF) of PD, MSA, CBD and PSP patients was assessed through an in-house nanoluciferase-based immunoassay. This study identified increased receptor processing in early-stage LBD within the PFC and striatum, key brain areas in neurodegeneration. In MSA only the 52 kDa form of GPR37 appeared in the striatum. This form was also significantly elevated in the striatum of AD necropsies. On the contrary, GPR37 processing remained unchanged in the brains of CBD and PSP patients. Furthermore, while CSF ecto-GPR37 increased in PD patients, its levels remained unchanged in MSA, CBD, and PSP subjects. Importantly, patients with PD with rapid progression of the disease did not have elevated ecto-GPR37 in the CSF, while those with slow progression showed a significant increase, suggesting a possible prognostic use of ecto-GPR37 in PD. This research underscores the distinctive processing and density patterns of GPR37 in neurodegenerative diseases, providing crucial insights into its potential role as an indicator of PD progression rates.

Neurodegenerative diseases (NDDs) consist of a spectrum of disorders characterised by the dysfunction and ongoing loss of neurons and neuronal networks in the central nervous system (CNS)[1]. Among these, Alzheimer's disease (AD) and Parkinson's disease (PD) are the most common NDDs, each with markedly different clinical manifestations[1,2]. PD shows significant clinical overlap with disorders characterised by atypical parkinsonism syndrome (APS), including multiple system atrophy (MSA), corticobasal degeneration (CBD), and progressive supranuclear palsy (PSP)[3]. However, patients with APS exhibit a poor response to levodopa and have a different prognosis compared to PD[3]. Therefore, the exploration of new biomarkers is

[1]Pharmacology Unit, Department of Pathology and Experimental Therapeutics, School of Medicine and Health Sciences, Institute of Neurosciences, University of Barcelona, 08907 L'Hospitalet de Llobregat, Spain. [2]Neuropharmacology & Pain Group, Neuroscience Program, Bellvitge Institute for Biomedical Research, 08907 L'Hospitalet de Llobregat, Spain. [3]Breast Cancer Clinical Research Unit, Centro Nacional de Investigaciones Oncológicas – CNIO, 28029 Madrid, Spain. [4]Laboratory of Molecular Neurobiology, Department of Medical Biochemistry and Biophysics, Karolinska Institutet, Stockholm, SE-17177, Sweden. [5]Department of Pathological Anatomy, Cellular Biology, Histology, History of Science, Legal and Forensic Medicine and Toxicology. Biomedical Research and Innovation Institute of Cadiz (INiBICA). University of Cádiz, 11002 Cádiz, Spain. [6]Memory and Aging Center, University of California, San Francisco, CA, 94158, USA. [7]Neurological disorders and neurogenetics Group, Neuroscience Program, Bellvitge Institute for Biomedical Research, 08907 L'Hospitalet de Llobregat, Spain. [8]Laboratory of Translational Neuropharmacology, Department of Clinical Neuroscience, Karolinska Institutet, Stockholm, SE-17177, Sweden. [9]Basic and Clinical Neuroscience, Institute of Psychiatry, Psychology and Neuroscience, King's College London, London, UK. ✉e-mail: per.svenningsson@ki.se; fciruela@ub.edu

Parkinson's Foundation

essential to accurately stratify NDD, particularly in the early stages, when diagnosis is the most challenging.

Neuropathologies of NDDs can be broadly classified into different groups based on the aggregated proteins present. For example, alpha-synucleinopathies are characterised by the presence of aggregated α-synuclein, mainly in neurons as observed in Lewy body diseases (LBD) such as PD, or in oligodendrocytes, as shown in MSA[4]. Tauopathies, including AD, CBD, and PSP, are characterised by tau aggregation in neurons and glia[5]. Despite the various neuropathological characteristics, they share certain mechanisms of neurodegeneration[6,7], often involving common aggregated proteins. Interestingly, evidence has linked α-synuclein to the pathophysiology of AD[8]. Therefore, providing a better understanding of these intricate mechanisms has the potential to pave the way for the development of new therapeutic strategies aimed at improving the treatment and diagnosis of NDDs.

G protein-coupled receptors (GPCRs) represent primary targets for numerous centrally acting drugs currently approved[9]. Although changes in the expression and function of specific GPCRs are documented in neurodegenerative conditions[10], it is important to note that orphan GPCRs remain relatively poorly investigated in the context of NDDs. GPCR 37 (GPR37) is an orphan GPCR expressed primarily in the CNS, specifically in the corpus callosum, cortex, striatum, and substantia nigra[11,12]. This receptor has gained attention for its potential involvement in neurodegenerative processes, particularly in PD. GPR37 is a substrate for parkin, an E3 ubiquitin ligase found mutated in patients with autosomal recessive juvenile PD[13]. The absence or overexpression of parkin has been associated with a higher propensity of GPR37 to misfold and aggregate, ultimately leading to cell death[14,15]. Furthermore, the N-terminal domain of GPR37 (ecto-GPR37) undergoes rapid and constitutive cleavage by ADAM-10[16,17], leading to the shedding of this ectodomain into the extracellular milieu. Recently, we reported higher levels of GPR37 protein density and mRNA expression in *post-mortem* substantia nigra samples from patients with sporadic PD[18].

To date, it is not clear whether the described GPR37 alterations are exclusive to PD or whether they extend to other conditions presenting similar symptoms (i.e., APS) or are associated with the same aggregated proteins (i.e., α-synuclein). Taking this into account, we conducted an evaluation of GPR37 processing and expression in the prefrontal cortex (PFC) and the striatum of individuals affected by different NDDs. The main objective was to determine whether GPR37 alterations could potentially serve as a reliable biomarker for PD.

Results

Expression of human GPR37 in PFC and striatum

The expression and possible role of GPR37 in neurodegeneration have not yet been fully elucidated. Consequently, our first aim was to identify the different subsets of cells expressing GPR37 in the human brain, specifically within the PFC and striatum, key areas in the pathogenesis of NDDs such as PD and AD. Taking advantage of existing single-cell mRNA sequencing datasets, we examined GPR37 mRNA expression in different cellular subpopulations of human PFC and striatum. Importantly, the datasets indicated elevated expression of GPR37 mRNA in cells expressing mature oligodendrocyte markers. In contrast, reduced expression was observed in excitatory neurons within the PFC (Fig. 1A) and in medium spiny neurons in the striatum (Fig. 1B). Limited expression was observed in astrocytes from both areas of the brain (Fig. 1A, B). In fact, moderate to low expression of GPR37 has been reported in neurons[12,14,15,19]. Given that it is highly expressed in myelinated brain tracts[12], we sought to establish whether the receptor is present in the cell soma or within the myelin sheath. To achieve this, we fractionated human brain tissue and myelin purification was validated by immunoblotting using the myelin marker (MAG) and the nuclear non-myelin marker (Olig-2) (Fig. 1C). In a crude tissue extract obtained from a pool of LBD PFC plus striatum necropsies, the anti-pan-GPR37-C antibody detected a GPR37 protein band pattern compatible with the putative precursor (67 kDa) and glycosylated (93 kDa) full-length (FL) receptor, as well as several cleaved forms of the N-terminus (52 kDa, 47 kDa, 43 kDa and 39–40 kDa) (Fig. 1C), as previously described in necropsies of substantia nigra[18]. Importantly, while a similar pattern of protein bands was observed in the non-myelin fraction, GPR37 was undetectable in the myelin-enriched fraction. In summary, these results suggest that although GPR37 is predominantly located in myelinated brain tracts[12], at the subcellular level, its presence is restricted to cell bodies. This localization is likely to have originated from oligodendrocytes but can also be derived from neurons or astrocytes.

Differential density of GPR37 in PFC and striatum necropsies of subjects with LBD and APS

A significant increase in both GPR37 mRNA expression and protein density was recently demonstrated in the substantia nigra of patients with sporadic PD[18]. Consequently, our objective was to assess whether this increase is observed in a similar way in the PFC and striatum, two areas of the brain commonly implicated in the pathogenesis of PD. To this end, we evaluated the density of GPR37 in necropsies of neurological controls and patients stratified within different Braak LBD stages. Interestingly, although the FL receptor form was not altered in the different Braak LBD stages analysed, the 39–47 kDa cleaved forms of the receptor exhibited a significant increase in both PFC ($P = 0.035$) and striatum ($P = 0.009$) in Braak stages 1/2 compared to NC (Fig. 2). Consequently, when all forms of GPR37 (that is, total) were considered, a significant increase in the density of GPR37 was observed in PFC ($P = 0.023$) and striatum ($P = 0.004$) only in the LBD1/2 stages (Fig. 2). Moreover, the 52 kDa form (black squares, Fig. 2), prevalent in PD SN necropsies[18] and limited in NC, was detected in some PFC and striatal samples of patients with LBD1/2 and LBD5/6, but not in the stages 3/4 (Supplementary Table 4). These results reinforce the notion that GPR37 processing is altered in the pathogenesis of LBD, especially in the early stages of the disease. Finally, we evaluated the density of ADAM-10, the metalloprotease involved in the cleavage of GPR37, in the same PFC and striatal necropsies. Two ADAM-10 species were identified by immunoblotting, the ~84 kDa immature (ProADAM-10) form and the ~65 kDa mature (active) form, as previously reported[20]. We found elevated density of mature or active ADAM-10, but not total, in the PFC of LBD 5/6 subjects compared to NC. However, in the other Braak stages analysed ADAM-10, both in total and active form, was not altered (Fig. 2).

APSs are less common neurological disorders with different underlying pathologies. Since these conditions show unique neuropathological characteristics, evaluating the expression and processing of GPR37 in APS could shed light on the role of GPR37 in neurodegenerative processes. To do this, we evaluated the density of GPR37 in the PFC and the striatum of necropsies of MSA, CBD, and PSP. In the PFC, while the expression of GPR37 was unchanged in MSA, CBD and PSP compared to NC, in MSA a significant increase in the density of the FL, 39–47 kDa forms and, consequently, the total amount of GPR37 was observed compared to the PSP group (Fig. 3A, B). On the contrary, in the striatum, when compared to NC, an up-regulation of the FL form of GPR37 was observed in patients with CBD ($P = 0.012$) and PSP ($P = 0.04$) (Fig. 3C, D). Interestingly, the 52 kDa form was identified in several MSA necropsies both in the PFC and striatum but was not detected in the CBD and PSP groups (Fig. 3; Supplementary Table 4). Regarding ADAM-10 expression, a significant reduction in the total density of the metalloprotease was found in the PFC of PSP subjects respect to NC ($P = 0.04$; Fig. 3). In contrast, the total expression of ADAM-10 was increased in the striatum of MSA ($P = 0.032$), CBD ($P = 0.049$) and PSP ($P = 0.043$) necropsies (Fig. 3). However, regarding the active form of ADAM-10, no differences were found in any of the APS conditions tested (Fig. 3). These results suggest that among the different APS necropsies evaluated, none of them showed altered processing of GPR37 neither in the PFC nor striatum.

Altered density of GPR37 and ADAM-10 in PFC and striatum necropsies of subjects with AD

Next, we evaluated possible alterations in the density of GPR37 and ADAM-10 in AD, the most prevalent neurodegenerative disorder. Here, we only

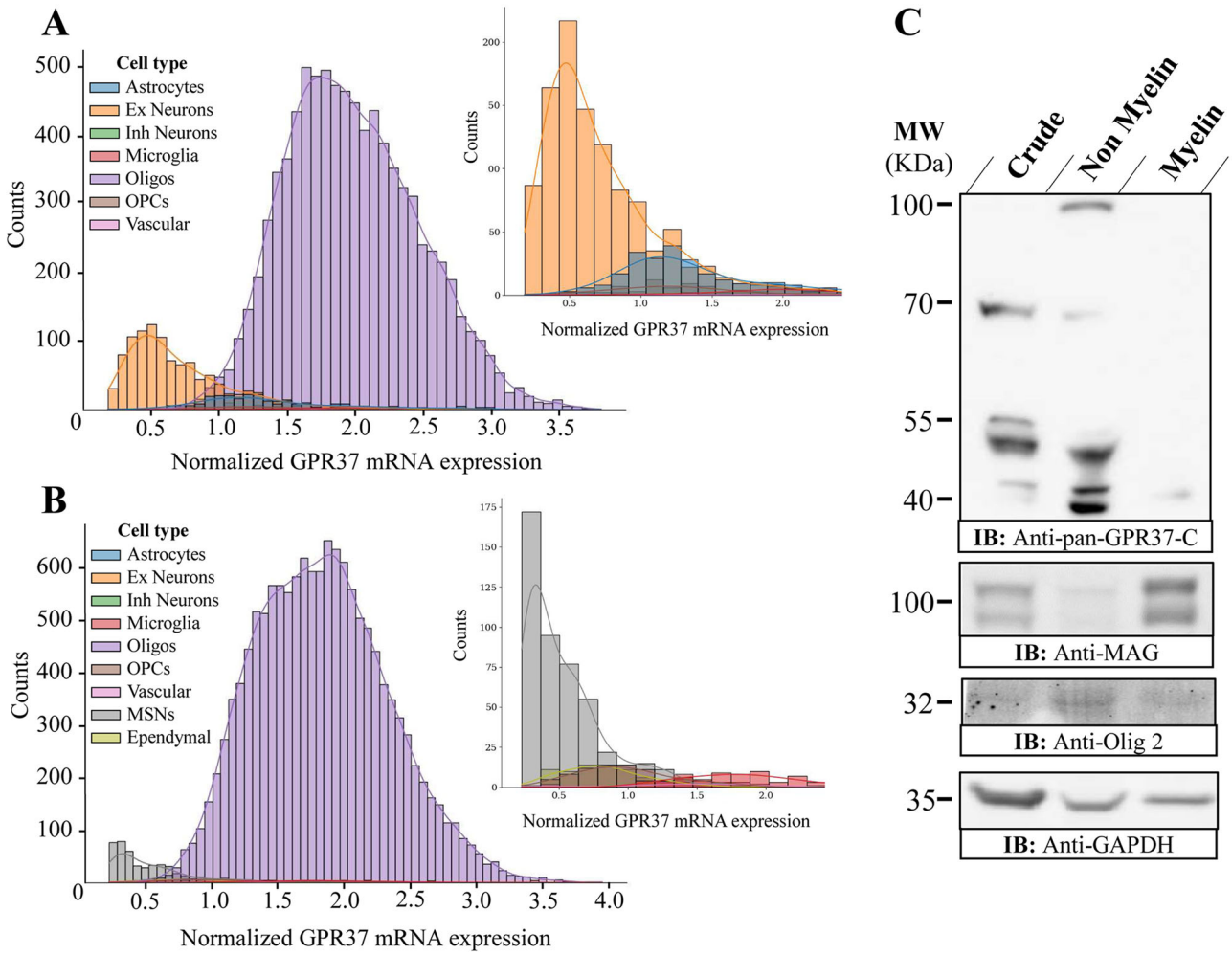

Fig. 1 | Expression of human GPR37 in the adult brain. Distribution of normalized GPR37 expression in the different populations in the prefrontal cortex (PFC) (**A**) and striatum (**B**) snRNA-seq dataset, excluding all nuclei with zero GPR37 expression. Data sets were obtained from 9 (**A**) and 8 (**B**) control subjects from two previous publications[33,37]. The x-axis represents the normalized and log-transformed mRNA expression of GPR37, while the y-axis represents the number of nuclei. The inset graph shows the same representation but excludes oligodendrocytes. Abbreviations: Excitatory neurons (Ex Neurons), inhibitory neurons (Inh Neurons), mature oligodendrocytes (Oligos), oligodendrocyte precursor cells (OPCs) and medium spiny neurons (MSNs). **C** Immunoblots showing the expression of GPR37, myelin associated glycoprotein (MAG), and Olig 2 in a sample of pooled human PFC and striatum. Myelin and non-myelin extracts were isolated by sucrose gradients and loaded into separate wells. The sample prior to the isolation process (crude) was also analysed. GAPDH was used to determine the amount of protein loaded into each well.

considered AD cases classified as Braak stages V and VI, as tau aggregation in these stages extends to the PFC and striatum[21]. Under the same experimental conditions, the 39–47 kDa forms of GPR37, and concomitantly the total density of the receptor, increased in the striatum (Fig. 4C, D), but not in the PFC (Fig. 4A, B). As shown with LBD and MSA samples, the 52 kDa form was observed both in the PFC and striatum of AD subjects (Fig. 4). In this case, the statistical analysis revealed that the 52 kDa band is significantly more detected only in the striatum of AD necropsies compared to NC ($P = 0.004$; Supplementary Table 4). These results suggest that the processing and density of GPR37 are differentially regulated in the PFC and striatum of AD patients. Subsequently, we evaluated ADAM-10 density. No changes were found in PFC (Fig. 4A, B), while the active form of ADAM-10 increased significantly ($P = 0.023$) in the striatum (Fig. 4C, D). Overall, AD striatal samples showed a unique parallelism between the density of the cleaved forms of GPR37 and the active form of ADAM-10, a phenomenon that was not observed in the other neurodegenerative conditions tested.

Ecto-GPR37 density in the CSF of subjects with Parkinsonism

The processing of GPR37 results in the release of its N-terminal domain into the extracellular environment[17]. This process becomes more pronounced in PD, suggesting that monitoring ecto-GPR37 levels could serve as a promising biomarker for the disease[18]. We interrogated whether ecto-GPR37 levels are also altered in NDDs other than PD. Therefore, we analysed the presence of ecto-GPR37 peptides in the CSF of patients with parkinsonism. To this end, we implemented our in-house nanoluciferase-based immunoassay[18] to quantify ecto-GPR37 in CSF samples from MSA, CBD, and PSP patients. We previously reported an increase in the concentration of ecto-GPR37 peptides in CSF samples from PD patients in two independent clinical cohorts, while it did not increase in CSF samples from AD subjects[18]. As shown in Fig. 5, ecto-GPR37 levels increased significantly in PD ($P = 0.023$), resulting in an average of 369 ± 58 pg/mL (Fig. 5A). The analysis of the ROC curve confirmed that the ecto-GPR37 in-house ELISA could differentiate PD patients from NCs, as previously reported[18], with an area under the curve (AUC) of 0.7 (0.535–0.871) ($P = 0.03$) (Fig. 5B). In this case, the technique, with a cut-off value of 230 pg/mL, had a sensitivity of 78% and a specificity of 65% (Fig. 5B). On the contrary, no changes in ecto-GPR37 levels were observed in APS (MSA, CBD and PSP) CSF samples (Fig. 5A). The corresponding ROC curve analysis showed that the ecto-GPR37 in-house ELISA could not discriminate between the NCs and MSA (AUC = 0.57, $P = 0.45$; Fig. 5C),

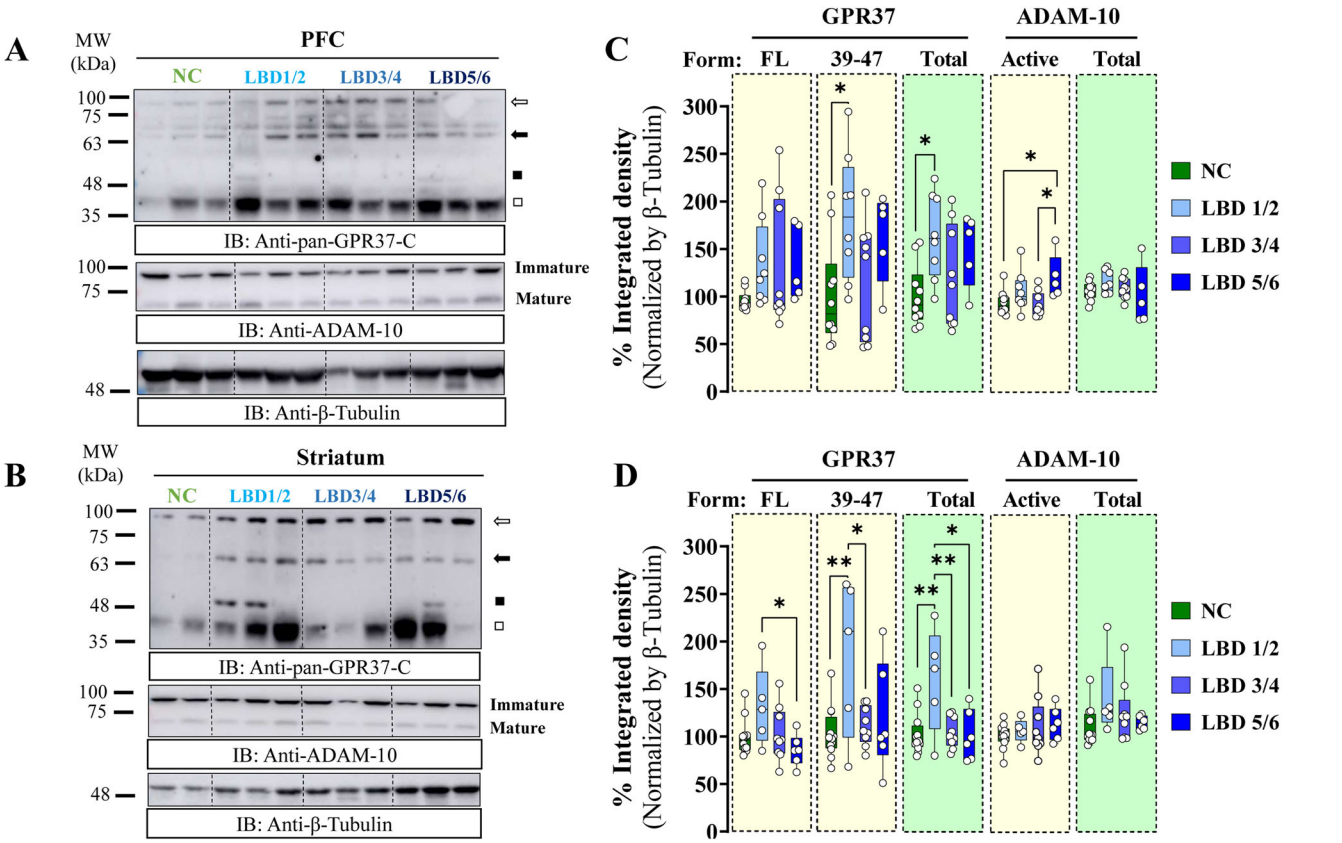

Fig. 2 | GPR37 and ADAM-10 protein density in Lewy Body disease post-mortem brain. Representative immunoblots showing the expression of GPR37 in the prefrontal cortex (PFC) (**A**) and striatum (**B**) of neurological controls (NC) and subjects with Lewy body disease (LBD) (Braak LBD stages 1/2, 3/4 and 5/6). Myelin was removed from samples and non-myelin extracts were analysed by SDS-PAGE and immunoblotted using antibodies against GPR37 and ADAM-10. Different GPR37 forms were identified including the full-length (FL; black arrow), post-translationally modified FL (white arrow) and GPR37 N-terminus cleaved forms (squares). Relative quantification of GPR37 and ADAM-10 protein density in the PFC (**C**) and striatum (**D**) of NC and LBD patients. For GPR37, the immunoblots corresponding to the FL (arrows) and 39–47 kDa (white square) forms were quantified by densiometric scanning. The sum of all receptor forms (total), including the 52 kDa form (black square), was also measured. For ADAM-10, the protein bands corresponding to the proADAM-10 (immature) and active (mature) forms of the protease were quantified by densiometric scanning. The levels of mature ADAM-10 were normalized by the total (immature + mature) ADAM-10 band density. Values were normalized to β-tubulin in each lane to correct for protein loading. Results are expressed as the percentage (mean ± SEM; $n = 5–12$ per group) of NC subjects. $^{*}P < 0.05$ $^{**}P < 0.01$, one-way ANOVA followed by Tukey's multiple comparison test.

CBD (AUC = 0.59, $P = 0.29$; Fig. 5D) or PSP (AUC = 0.57, $P = 0.42$; Fig. 5E) subjects.

Subsequently, we investigated how the progression rate of PD affected ecto-GPR37 levels. Importantly, CSF ecto-GPR37 levels in samples obtained at the onset of the disease were significantly higher in patients with PD progressing slowly compared to NC ($P = 0.002$) or patients with PD progressing rapidly ($P = 0.001$). These results indicate a possible role for GPR37 processing in the progression rate of PD (Fig. 6A). ROC curve analysis showed that the ecto-GPR37 in-house ELISA could discriminate between patients with PD who progress slowly and NC (AUC = 0.83, $P = 0.005$, Fig. 6B) or patients with PD who progress rapidly (AUC = 0.85, $P = 0.003$, Fig. 6D). In contrast, the ecto-GPR37 in-house ELISA could not differentiate between subjects with NC and PD progressing rapidly (AUC = 0.55, $P = 0.627$), as shown in Fig. 6C. These results indicate the potential utility of ecto-GPR37 levels as a predictive biomarker of the progression rate in PD.

Discussion

The N-terminal domain of GPR37 undergoes metalloprotease cleavage, leading to ectodomain shedding into the extracellular environment while retaining several cleaved receptor forms at the cell surface[17,18]. To better understand the potential molecular alterations associated with GPR37 in neurodegeneration, we evaluated the total density and relative prevalence of the various processed forms of membrane receptors in a collection of brain necropsies from NDD. Additionally, we evaluated ecto-GPR37 levels in CSF using a novel in-house ELISA method. Our study reveals differential processing and expression patterns of GPR37 within the different NDDs analyzed, likely occurring in oligodendrocytes, and possibly also in neurons or astrocytes of the PFC and the striatum. Importantly, we uncover that ecto-GPR37 increased significantly only in patients with a slow progression of PD, suggesting a potential role as a predictive biomarker of the disease progression rate.

In a healthy individual, the different forms of GPR37 identified by immunoblotting in the PFC and striatum were consistent with those previously reported in the substantia nigra (i.e., FL and 39–47 kDa)[18], with no age-dependent affectation (Supplementary Fig. 2). Similarly, in some LBD necropsies, the receptor forms detected (i.e., FL, 52 kDa, and 39–47 kDa) closely correlated with those observed in the substantia nigra of individuals with PD[18]. These findings suggest a comparable post-translational processing of GPR37 in these regions of the brain, both under normal and disease conditions. Interestingly, the 52 kDa receptor form, nearly absent in NC, was detected in the early stages of the disease (i.e., LBD1/2) in both the PFC and striatum. Furthermore, the 39–47 kDa form, more conspicuously present in NC, also increased only in LBD1/2. These results, which reinforce the idea that GPR37 density and processing are altered within the pathogenesis of LBD, point toward a disease stage-dependent processing of GPR37 in LBD. Early neurodegenerative events involve inflammatory processes and impaired autophagy and dopaminergic neurotransmission[22]. Importantly, GPR37 has been associated with all these processes[19,23–25],

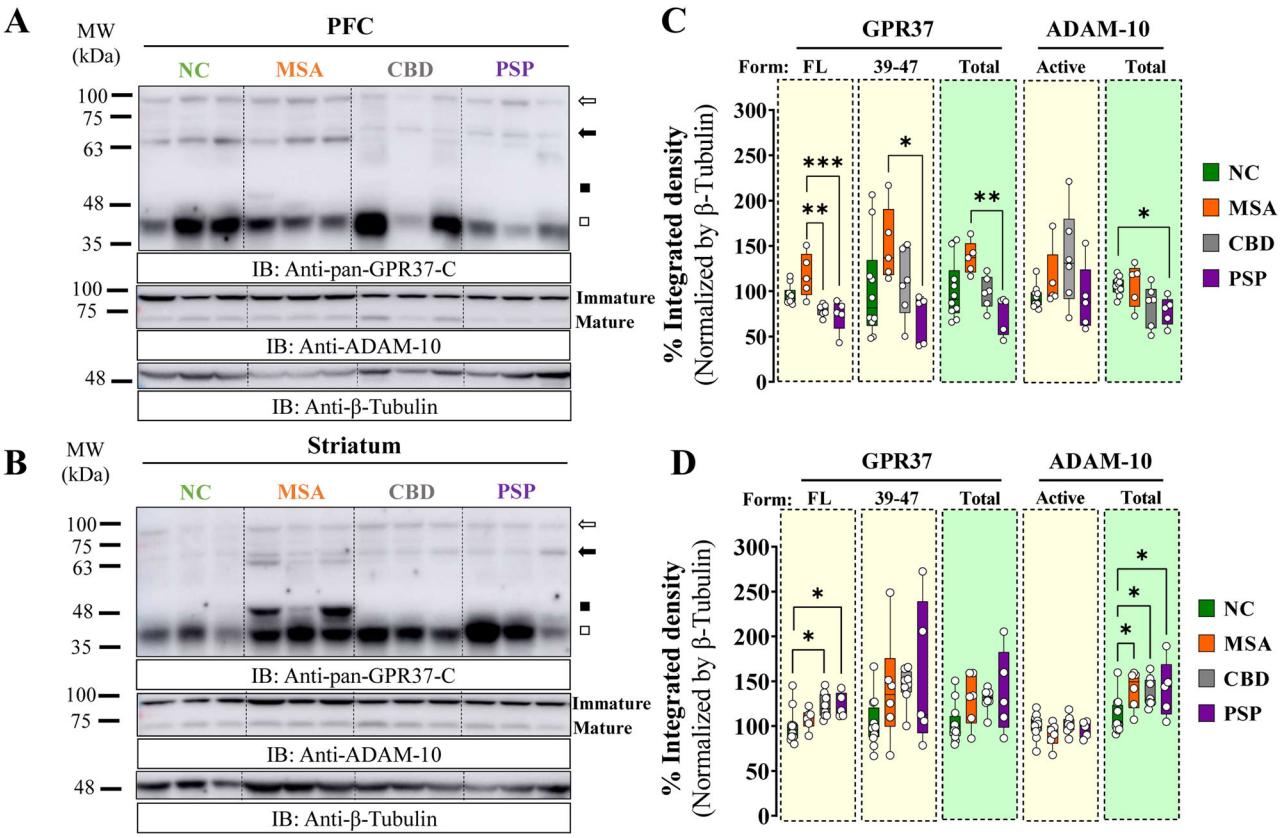

Fig. 3 | GPR37 and ADAM-10 protein density in atypical parkinsonism post-mortem brain. Representative immunoblots showing the expression of GPR37 in the prefrontal cortex (PFC) (**A**) and striatum (**B**) of neurological controls (NCs) and patients with multiple system atrophy (MSA), corticobasal degeneration (CBD) and progressive supranuclear palsy (PSP). Myelin was removed from samples and non-myelin extracts were analysed by SDS-PAGE and immunoblotted using antibodies against GPR37 and ADAM-10. Different GPR37 forms were identified including the full-length (FL; black arrow), post-translationally modified FL (white arrow) and GPR37 N-terminus cleaved forms (squares). Relative quantification of GPR37 and ADAM-10 protein density in the PFC (**C**) and striatum (**D**). For GPR37, the immunoblots corresponding to the FL (arrows), and 39–47 kDa (white square) forms were quantified by densiometric scanning. The sum of all receptor forms (Total) including the 52 kDa form (black square) was also measured. For ADAM-10, the protein bands corresponding to the proADAM-10 (immature) and active (mature) forms of the protease were quantified by densiometric scanning. The levels of mature ADAM-10 were normalized by the total (immature + mature) ADAM-10 band density. Values were normalized to β-tubulin in each lane to correct for protein loading. Results are expressed as the percentage (mean ± SEM; $n = 5–12$ per group) of the NC. $^{*}P < 0.05$ $^{**}P < 0.01$ $^{***}P < 0.001$, one-way ANOVA followed by Tukey's multiple comparison test.

suggesting the involvement of the receptor in molecular events occurring during early deposition of LB in the PFC and striatum.

Within APS, GPR37 processing was not significantly altered in any condition tested. However, it is worthy to mention that the 52 kDa form was detected in a substantial number of MSA samples. However, unlike LBD1/2, no increase was observed in the conspicuous 39–47 kDa form. Interestingly, MSA, unlike PD, is characterised by the aggregation of α-synuclein in oligodendrocytes rather than in neurons[26]. Therefore, our results suggest that the high expression of GPR37 in oligodendrocytes may be related to α-synuclein aggregation and the concomitant appearance of only the 52 kDa receptor form. In the context of the tauopathies tested, although this 52 kDa receptor form was not found in any subject affected by CBD and PSP, in AD, it was detected in the PFC and increased significantly in the striatum compared to NC. Interestingly, AD stands out as the only tauopathy linked to α-synuclein. Numerous postmortem and clinical evidence support the role for α-synuclein in the pathophysiology of AD[8]. However, the extent and significance of α-synuclein involvement in AD remain a subject of investigation. Therefore, our results suggest that up-regulation of the 52 kDa receptor form in AD may be related to α-synuclein aggregation rather than tau accumulation. Alternatively, since AD, from the taupathologies analysed, is the only one characterised by extracellular accumulations of misfolded Aβ-amyloid[27], we can rule out that upregulation of the 52 kDa receptor form in AD is more related to Aβ-amyloid plaques. Interestingly, previous reports have shown that GPR37 mRNA expression levels are not altered in the PFC of AD patients[18]. We did not observe significant differences in the total density of the GPR37 protein in the PFCs of AD patients. However, AD patients showed an increase in total GPR37 expression in the striatum, likely sustained by a concomitant increase in density in the conspicuous 39–47 kDa form, as it occurs in subjects with PD. Transcriptional studies comparing striatal changes between AD and PD revealed that microglial activation was largely unique to each disorder and associated with amyloid pathology[28]. This suggests an indirect association between GPR37 expression and neuroinflammation that needs to be fully elucidated. Finally, it is intriguing that the total density of GPR37 was specifically increased in the striatum from CBD and PSP patients. Whether GPR37 is related to the cognitive and behavioural changes associated with these diseases is something that needs to be explored in more detail. Collectively, these results suggest a different brain region and disease-associated processing of the N-terminus of GPR37 in neurodegeneration. Therefore, the presence of the 52 kDa form of GPR37 in the striatum of LBD, MSA and AD constitutes a distinctive fingerprint of GPR37 processing in these neurodegenerative conditions. On the contrary, the increase in density of the 39–47 kDa GPR37 form was found in the PFC and the striatum of LBD1/2, while in AD the increase was observed only in the striatum, indicating a region-dependent control of GPR37 expression and processing within these NDD. In fact, ADAM-10 initial cleavage of FL GPR37 forms generates the 52 kDa

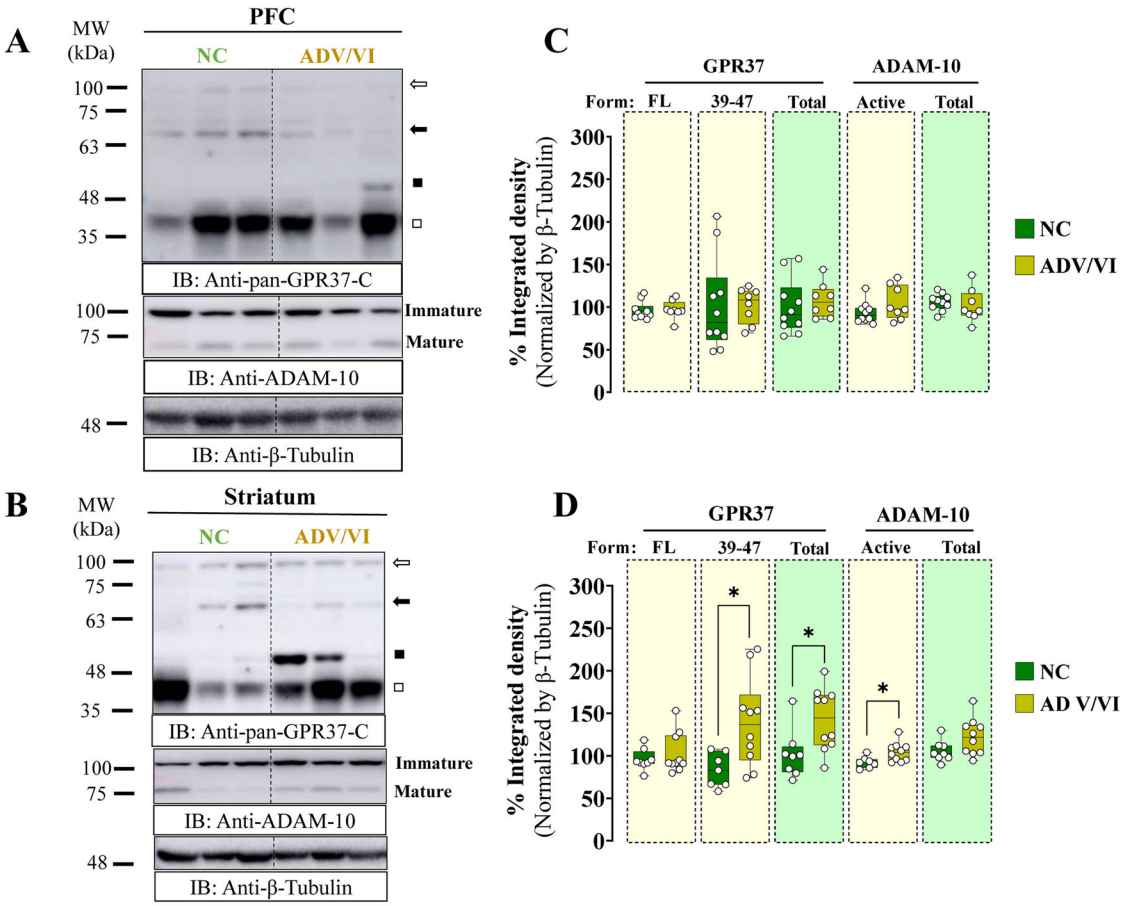

Fig. 4 | GPR37 and ADAM-10 protein density in Alzheimer's disease post-mortem brain. Representative immunoblots showing the expression of GPR37 in the prefrontal cortex (PFC) (**A**) and striatum (**B**) of neurological controls (NCs) and Alzheimer's disease (AD) patients (Braak AD stage V/VI). Myelin was removed from samples and non myelin extracts were analysed by SDS-PAGE and immunoblotted using antibodies against GPR37 and ADAM-10. Different GPR37 forms were identified including the full-length (FL; black arrow), post-translationally modified FL (white arrow) and GPR37 N-terminus cleaved forms (squares). Relative quantification of GPR37 and ADAM-10 protein density in the PFC (**C**) and striatum (**D**). For GPR37, the immunoblots corresponding to the FL (arrows), and 39–47 kDa (white square) forms were quantified by densiometric scanning. The sum of all receptor forms (total), including the 52 kDa form (black square), was also measured. For ADAM-10, the protein bands corresponding to the proADAM-10 (immature) and active (mature) forms of the protease were quantified by densiometric scanning. The levels of mature ADAM-10 were normalized by the total (immature + mature) ADAM-10 band density. Values were normalized to β-tubulin in each lane to correct for protein loading. Results are expressed as the percentage (mean ± SEM; PFC: $n = 5$ per group; Striatum: $n = 8–10$ per group) of the NC. $^*P < 0.05$ vs NC, Student's t test.

form[16,17], and further processing of the 52 kDa form by metalloproteinases may end with fuelling of the 39–47 kDa GPR37 form; however, this should be further demonstrated.

ADAM-10, known for its role in cleaving amyloid-β precursor protein, has demonstrated the capacity to decrease the formation of Aβ-amyloid plaques[29]. Furthermore, ADAM-10 is associated with beneficial effects on tau pathology, preservation of normal synaptic functions, and maintenance of neuronal network homeostasis[29]. Significantly, we reveal a distinctive alteration in ADAM-10 density, specifically an increase in its active form, exclusively within the striatum of AD subjects. This observation was strongly correlated with an increase in the density of 39–47 kDa forms of GPR37. It could be speculated that the increase in the density of the active form of ADAM-10 in the striatum is related to a compensatory mechanism to slow the progression of the disease. This contention might be supported by the observation that ADAM-10 levels in plasma from AD subjects are increased[30]. However, the existence of contradictory results on ADAM-10 levels in the CSF of AD patients[30] underscores the need for a further detailed interpretation of the increased activity of ADAM-10 within the brain of AD, for example, compared to PD.

Higher levels of ecto-GPR37 have recently been shown in the CSF of patients with PD[18]. Again, here we report increased levels of ecto-GPR37 in an independent cohort of PD patients. Interestingly, ecto-GPR37 peptides increased only in patients with slow progressing PD, suggesting that ecto-GPR37 levels could predict the progression rate of PD as rapid or slow. Furthermore, increased levels of ecto-GPR37 only in patients with PD that progress slowly may suggest that these peptides have neuroprotective properties, potentially reducing the progression of the disease. Finally, we speculate that these ecto-GPR37 peptides, rather than being inert, may function as modulators of certain cell responses, such as inflammation, adhesion, migration, and proliferation, as documented for other cell surface proteins[31]. Confirmation of ecto-GPR37 peptides as autocrine or paracrine modulators could open new avenues for considering these peptides as therapeutic targets in diverse pathologies, including NDD.

This study faces several limitations, mainly due to the relatively small number of NDD samples. To mitigate heterogeneity within the necropsies used in immunoblot experiments, we excluded samples with comorbidities. Furthermore, although the cohorts used to detect ecto-GPR37 in CSF were moderately large, some variability was observed in the in-house ELISA assay. Despite these challenges, our study, which relied on well-preserved necropsies without comorbidities and CSF samples from patients rigorously diagnosed, has yielded valuable insights. Therefore, it will be essential to corroborate these findings through independent sample collections for robust validation.

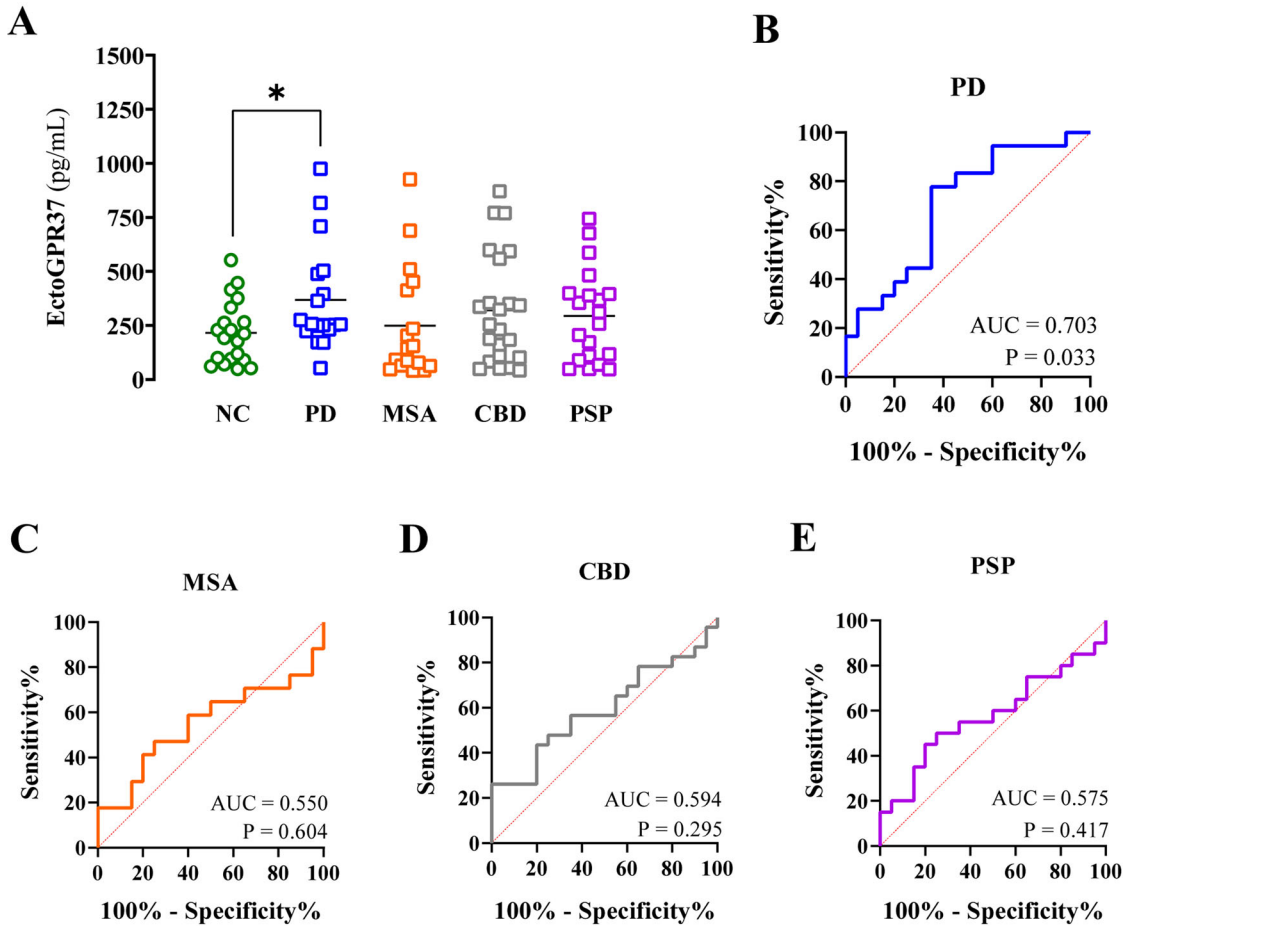

Fig. 5 | Determination of ecto-GPR37 in CSF of patients with parkinsonism. **A** Screening of ecto-GPR37 levels in cerebrospinal fluid (CSF) from neurological controls (NCs) and patients with Parkinson's disease (PD), multiple system atrophy (MSA), corticobasal degeneration (CBD) and progressive supranuclear palsy (PSP). $^{*}P < 0.05$ vs NC, Student's t-test. ROC curve analysis of CSF ecto-GPR37 comparing NC with PD (**B**), MSA (**C**), CBD (**D**) and PSP (**E**) subjects. The Area Under the Curve (AUC) and the *p*-value is indicated for each ROC curve.

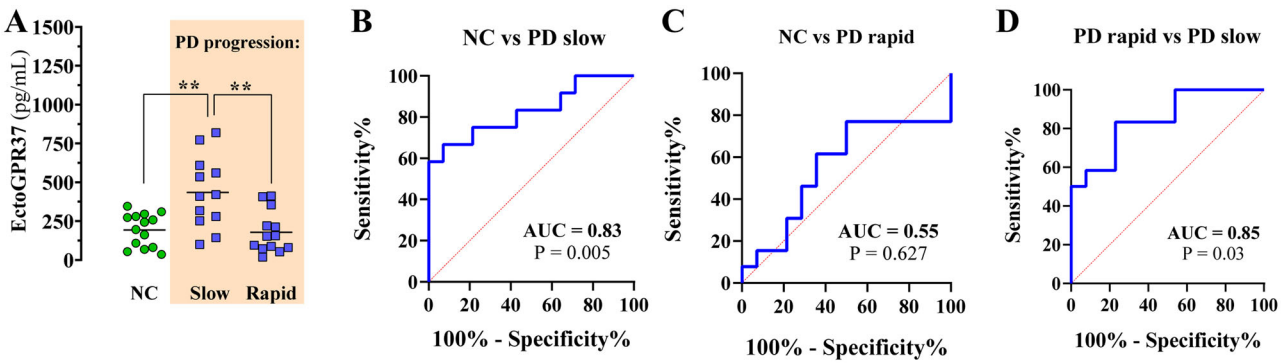

Fig. 6 | Determination of ecto-GPR37 in CSF of patients with Parkinson's disease. **A** Concentration of ecto-GPR37 peptides in cerebrospinal fluid (CSF) from neurological controls (NCs) and patients with Parkinson's disease (PD) patients with slow or rapid disease progression. $^{**}P < 0.01$, one-way ANOVA followed by Tukey's multiple comparison test. ROC curve analysis of CSF ecto-GPR37 comparing NC and PD slow (**B**) or PD rapid (**C**) and PD slow and rapid between them (**D**). The Area Under the Curve (AUC) and the *p*-value is indicated for each ROC curve.

Methods

Antibodies

The following antibodies were used to detect proteins of interest: rabbit anti-human-GPR37-N polyclonal antibody[18,32], rabbit anti-pan-GPR37-C polyclonal antibody[12,18], mouse anti-MAG monoclonal antibody (sc-166849, 1:1000, Santa Cruz Biotechnology Inc., Dallas, TX), rabbit anti-Olig2 polyclonal antibody (ab109186, 1:2000, Abcam Inc., Cambridge, UK), rabbit anti-ADAM-10 monoclonal antibody (ab124695, 1:2000, Abcam, Cambridge, UK), mouse anti-GAPDH monoclonal antibody (97166, 1:1000, Cell Signaling Technology, Massachusetts, US) and rabbit anti-β-tubulin polyclonal antibody conjugated to horseradish peroxidase (HRP) (ab21058, 1:2000, Abcam, Cambridge, UK). For immunoblot analysis, the

following secondary antibodies were used: HRP-conjugated goat anti-rabbit IgG (11829140; 1:30.000; Fisher Scientific, Massachusetts, US), HRP-conjugated goat anti-mouse IgG (10158113; 1:10.000; Fisher Scientific, Massachusetts, US), 680RD dye-conjugated goat anti-mouse IgG (926-68070; 1:10.000; LI-COR, Nebraska, US) and 800CW dye-conjugated goat anti-rabbit IgG (926-32211; 1:10.000; LI-COR, Nebraska, US).

Transcriptomic data access and processing

Two single nuclei RNA sequencing (snRNA-seq) datasets with accession numbers GSE157827 and GSE152058 from were retrieved from the Gene Expression Omnibus (GEO, https://www.ncbi.nlm.nih.gov/geo/). These datasets originated from previous studies on neurodegenerative disorders on the PFC and the striatum and included both pathological and control subjects[33]. For our purposes, we kept only the nuclei belonging to control individuals. On both datasets, scrublet[34] was used to detect putative doublets and we employed Scanpy[35] to apply quality control filters based on the distribution of counts and genes found on each dataset (Supplementary Table 1). Then, the data was normalized to 10000 counts per cell and log-transformed. The striatum dataset contained cell type annotations, whereas in the PFC data we performed dimensionality reduction and clustering, and then assigned cell-type labels based on sets of known marker genes (Supplementary Table 2). On the human PFC dataset from Lau et al.[33], we found 83932 nuclei from control subjects. Using scrublet[34], 4910 putative doublets were detected and removed. The rest of the nuclei were filtered according to their total counts and genes and their fraction of mitochondrial content. Data from 78863 nuclei were retained, which we then normalised and log-transformed. Principal component analysis (PCA) was applied, retaining the first 18 principal components (PCs). Data were clustered in the PCA space using the Louvain algorithm[36] with a resolution of 0.2. Clusters were labelled according to the expression of bona-fide markers for the main cell types in the PFC. The dataset of the human striatum from Lee et al.[37] contained 69551 nuclei from control subjects, already filtered by counts and genes. When scrublet was applied, 38 putative doublets were removed, and 14 nuclei with more than 15% mitochondrial content were also left out. The cells were labelled by the original authors, thus the expression of GPR37 was directly observed on the different cell types. The number of subjects used in the analysis, as well as their age and gender, are described in Supplementary Table 3.

Human post-mortem brain samples

Human *post-mortem* brain tissues were obtained from the HUB-ICO-IDIBELL Biobank, the Hospital Clinic-IDIBAPS Biobank, the Biobank Unit of Navarrabiomed research center and Queens Square Brain bank London following the guidelines of Spanish, UK, and Swedish legislation on this matter (Real Decreto de Biobancos 1716/2011; Regional Ethics Review Board of Stockholm (2014/1366-31))[38,39] and upon approval of the local ethics committees. A hemisphere was immediately cut into 1 cm thick coronal sections, and selected areas of the encephalon were rapidly dissected, frozen on metal plates over dry ice, placed in individual air-tight plastic bags, and stored at −80 °C until use for biochemical studies. The other hemisphere was fixed by immersion in 4% buffered formalin for 3 weeks for morphological studies. The neuropathological diagnosis of all cases was made based on the evaluation of 20 selected de-waxed paraffin sections containing regions of the cerebral cortex, diencephalon, thalamus, brain stem and cerebellum, which were stained with haematoxylin, eosin, and Klüver-Barrera. Pathological cases were classified as MSA, CBD, PSP, AD and LBD at stages 1-6 according to the nomenclature of Braak et al.[40,41]. For AD, only cases classified as stages V and VI were considered. The middle-aged control cases had not suffered from neurological, psychiatric, or metabolic diseases (including metabolic syndrome), and did not have abnormalities in the neuropathological examination except vascular disease and hypoxia. Cases with associated pathologies such as infections of the nervous system, brain neoplasm, systemic and central immune diseases, and metabolic syndrome were excluded from the present study. The selected brain areas were PFC Brodmann area 8 and striatum (caudate and putamen), and different series of samples (i.e. NCs, Braak LBD stage 1/2, Braak LBD stage 3/4, Braak LBD stage 5/6, Braak AD stage V/VI, MSA, CBD and PSP) were prepared according to their experimental use: (i) PFC immunoblotting: 10 NCs (9 males and 1 female; mean age: 60 ± 10 years), 8 Braak LBD stage 1/2 (7 males and 1 female; mean age: 75 ± 6 years), 9 Braak LBD stage 3/4 (6 males and 3 females; mean age: 72 ± 7 years), 5 Braak LBD stage 5/6 (4 males and 1 female; mean age: 76 ± 1 year), 5 MSA (2 males and 3 females; mean age: 63 ± 7 years), 6 CBD (5 males and 1 female; mean age: 73 ± 7 years) 5 PSP (3 males and 2 females; mean age: 75 ± 6 years), and 8 Braak AD stage V/VI (4 males and 4 females; mean age: 79 ± 5 years) cases; ii) NC, LBD, MSA, CBD and PSP striatum immunoblotting: 12 NCs (9 males and 3 females; mean age: 64 ± 17 years), 5 Braak LBD stage 1/2 (4 males and 1 female; mean age: 78 ± 5 years), 9 Braak LBD stage 3/4 (7 males and 2 females; mean age: 73 ± 9 years), 6 Braak LBD stage 5/6 (4 males and 2 females; mean age: 81 ± 3 years), 6 MSA (4 males and 2 females; mean age: 60 ± 7 years) and same CBD and PSP cases that for PFC; iii) AD striatum immunoblotting: 8 NCs (6 males and 2 females; mean age: 70 ± 21 years), and 10 Braak AD stage V/VI (5 males and 5 females; mean age: 79 ± 11 years) cases.

Participants providing CSF

PD, MSA, CBD and PSP patients were recruited at the movement disorders clinic at the Karolinska University Hospital Clinic, Sweden. CBD and PSP patients were also recruited from the Memory and Aging Center, University of California, USA. Patients underwent a clinical examination (including ratings of motor, cognitive and psychiatric symptoms) by an experienced neurologist (Supplementary Table 3). All included patients were longitudinally followed and the diagnosis of PD, including subsequent response to dopaminergic therapy, was confirmed before they were included in the CSF analysis. Therefore, the patients with PD satisfied the clinical diagnosis of PD according to the UK Parkinson's Society Brain Bank diagnostic criteria. Motor symptoms were evaluated with the Unified Parkinson's Disease Scale (UPDRS) part 3 in the ON state of the medication cycle. Non-motor and motor symptoms in daily activities were evaluated with UPDRS part 1 and part 2, respectively. UPDRS part 4 was used to measure motor complications[42]. Almost all patients had available scores for the Hoehn & Yahr scale assessing motor impairment[43], and 66% of the patients had available Montreal Cognitive Assessment scores (MoCA) assessing cognitive impairment[44]. In addition, within the routine visit self-evaluation questionnaires were implemented, including Non-Motor Symptoms Questionnaire[45], and Hospital Anxiety and Depression scale[46]. Finally, the medications were presented as L-dopa equivalent doses (LED)[47]. MSA, PSP and CBD patients were diagnosed based in current criteria[48–50]. Control subjects of the same age and sex were recruited from routine neurology examinations. Control patients were also recruited at the Karolinska University Clinic, Huddinge, Sweden and were diagnosed with benign neurological diagnoses, such as tension headache without evidence of dementia, no cognitive complaints, no PD, or other brain disease, and thus were defined as NCs.

CSF sample measurements

To determine ecto-GPR37 levels in humans, we used CSF samples from 18 PD, 17 MSA, 23 CBD, 20 PSP and 20 age- and sex-matched control patients (Supplementary Table 3). CSF samples were obtained by lumbar puncture from participants of the Karolinska University Clinic, collected in polypropylene tubes and immediately centrifuged at 1800 g at 4 °C for 10 min before being stored in aliquots of 100 µl at −80 °C as previously described[18].

For the analysis of CSF ecto-GPR37 in PD patients with slow (PD slow) and rapid (PD rapid) disease progression, 12 PD slow, 13 PD rapid and 14 age- and sex-matched control participants (Supplementary Table 5) were enrolled at the Karolinska University Hospital Clinic, Sweden. The control participants were those diagnosed with non-primarily neurodegenerative neurological and psychiatric diseases. All the participants had given written consent for the use of their clinical data and CSF for research purposes, and the study was approved by the regional ethics committee for medical

research in Stockholm (2011/500–31/1 and 2012/2224–32/4). All procedures followed were in accordance with the ethical standards indicated by the Declaration of Helsinki of 1975, as revised in 2000.

Brain membrane extract preparation

Postmortem human brain samples (~ 100 mg of PFC or striatum) were homogenised in 5 ml of ice cold 0.32 M sucrose solution supplemented with a protease inhibitor cocktail (Roche Molecular Systems, Pleasanton, CA, USA) using a Teflon homogeniser for 3 x 10 s on ice. The homogenate (Crude) was overlayed on 6 ml of 0.85 M sucrose solution in a Beckman centrifuge tube (Ultra-clear, 14 × 89 mm, Beckman Coulter Inc., California, US). The samples were then ultracentrifuged at 75,000 g for 30 min at 4 °C. The myelin fraction appeared in the interphase between both sucrose solutions, and the pellet contained the non-myelin fraction of the sample. Myelin fraction was transferred to a new tube, washed with 1 ml of sterile miliQ H_2O and resuspended in ice cold Tris buffer containing 50 mM Tris-Base (pH = 7.2) and a protease inhibitor cocktail (Roche Molecular Systems, Pleasanton, CA). The non-myelin fraction was resuspended with ice cold Tris buffer and homogenised by sonication on ice for 3 x 10 s. The samples were then centrifuged at 1000 g for 10 min at 4 °C and the supernatant was recovered and centrifuged at 12,000 g for 30 min at 4 °C. The pellet containing the membrane extracts of the non-myelin fraction was resuspended with Tris 50 mM buffer. Protein concentration of both fractions (myelin and non-myelin) was determined using the BCA protein assay kit (ThermoFisher Scientific) and 50 µg of protein were used for immunoblotting.

Gel electrophoresis and immunoblotting

Sodium dodecyl sulphate-polyacrylamide gel electrophoresis (SDS/PAGE) was performed using 10% polyacrylamide gels. Membrane extracts were loaded into gel wells, transferred to polyvinylidene difluoride membranes using a semidry transfer system (Bio-Rad, Hercules, CA, USA) and immunoblotted using the corresponding antibodies. Primary antibodies were detected using secondary antibodies conjugated with HRP or fluorescent dyes (see section Antibodies). HRP immunoreactive bands were developed using a chemiluminescent detection kit (Thermo Fisher Scientific, Waltham, MA, USA). The chemiluminescence and fluorescence signal was detected with an Amersham Imager 600 (GE Healthcare Europe GmbH, Barcelona, Spain) or a ChemiDoc Imaging System (12003154, Bio-Rad, California, US). The specificity of the rabbit anti-pan-GPR37-C polyclonal antibody and the rabbit anti-human-GPR37-N polyclonal antibody were validated using extracts from cells expressing human GPR37 (Supplementary Fig. 1).

Ecto-GPR37 detection in CSF

CSF ecto-GPR37 was measured with our home-made competitive ELISA method, as previously described[18]. Briefly, 96 wells / plate coated with streptavidin (ThermoFisher Scientific) were blocked with serum-free DMEM medium (100 µL/well) for 1 h at 22 °C. After three washes with ELISA buffer (25 mM Tris-base, 150 mM NaCl, 0.1% BSA, 0.05% Tween-20, pH = 7.2), wells were coated with 100 µL/well of anti-rabbit IgG biotin antibody (Sigma-Aldrich; 10 µg/mL in ELISA buffer) for 2 h at 22 °C. Subsequently, the wells were washed three times with ELISA buffer and 100 µL/well of anti-human GPR37-N antibody (1 µg/mL in ELISA buffer) were incubated for 2 h at 22 °C. At this point, 5 µL/well of CSF samples diluted with 45 µL/well of ELISA buffer were incubated overnight at 4 °C in a humid chamber. The following day, plates were washed three times with ELISA buffer and incubated with 50 µL of purified human ecto-GPR37^{NL} (100.000 relative light units [RLU]/µL in ELISA buffer) for 1 h at 22 °C in the dark. Finally, plates were washed three times with ELISA buffer and 90 µL of ELISA buffer was added to each well. Then 10 µL/well of 20 µM coelenterazine 400a solution (NanoLight Technologies, Pinetop, AZ; in ELISA buffer) was added. After 5 min of incubation, luminescence was measured using a CLARIOstar Optima plate reader (BMG Labtech GmbH, Ortenberg, Germany) and the output luminescence was reported as the integral RLU. Furthermore, a standard curve was generated using known concentrations of human ecto-GPR37^{SNAP}. Both the ecto-GPR37^{NL} and ecto-GPR37^{SNAP} products were purified from human embryonic kidney (HEK)-293 T cells, as previously detailed[18].

Statistics

Data are represented as mean ± standard error of mean (SEM). The number of samples (n) in each experimental condition is indicated in the corresponding figure legend. Outliers were evaluated using the ROUT method[51] assuming a Q value of 1% on GraphPad Prism 9 (San Diego, CA, USA). No outliers were found. Data normality was assessed using the Shapiro-Wilk normality test. Comparisons among experimental groups were performed by Student's t-test, one-way ANOVA with Dunnett's or Tukey's post-hoc test and ROC curve analysis using GraphPad Prism 10.1.0 (San Diego, CA, USA), as indicated. Statistical difference was accepted when $P < 0.05$.

Data availability

Data will be given upon request.

Received: 11 February 2024; Accepted: 27 August 2024;
Published online: 10 September 2024

References

1. Zaib, S. et al. Neurodegenerative diseases: their onset, epidemiology, causes and treatment. *Chem. Sel.* **8**, e202300225 (2023).
2. Gammon, K. Neurodegenerative disease: brain windfall. *Nature* **515**, 299–300 (2014).
3. Erkkinen, M. G., Kim, M. O. & Geschwind, M. D. Clinical neurology and epidemiology of the major neurodegenerative diseases. *Cold Spring Harb. Perspect. Biol.* **10**, a033118 (2018).
4. Coon, E. A. & Singer, W. Synucleinopathies *CONTINUUM Lifelong Learn. Neurol.* **26**, 72–92 (2020).
5. Saha, P. & Sen, N. Tauopathy: A common mechanism for neurodegeneration and brain aging. *Mech. Ageing Dev.* **178**, 72–79 (2019).
6. Foguem, C. & Kamsu-Foguem, B. Neurodegeneration in tauopathies and synucleinopathies. *Rev. Neurol. (Paris)* **172**, 709–714 (2016).
7. Bourdenx, M. et al. Protein aggregation and neurodegeneration in prototypical neurodegenerative diseases: Examples of amyloidopathies, tauopathies and synucleinopathies. *Prog. Neurobiol.* **155**, 171–193 (2017).
8. Twohig, D. & Nielsen, H. M. α-synuclein in the pathophysiology of Alzheimer's disease. *Mol. Neurodegener.* **14**, 23 (2019).
9. Sriram, K. & Insel, P. A. G protein-coupled receptors as targets for approved drugs: How many targets and how many drugs? *Mol. Pharm.* **93**, 251–258 (2018).
10. Wong, T. S. et al. G protein-coupled receptors in neurodegenerative diseases and psychiatric disorders. *Sig. Transduct Target Ther.* **8**, 177 (2023).
11. Marazziti, D. et al. Cloning of GPR37, a gene located on chromosome 7 encoding a putative g- protein-coupled peptide receptor, from a human frontal brain EST library. *Genomics* **45**, 68–77 (1997).
12. Morató, X. et al. The Parkinson's disease-associated GPR37 receptor interacts with striatal adenosine A2A receptor controlling its cell surface expression and function in vivo. *Sci. Rep.* **7**, 9452 (2017).
13. Murakami, T. et al. Pael-R Is Accumulated in Lewy Bodies of Parkinson's Disease. *Ann. Neurol.* **55**, 439–442 (2004).
14. Imai, Y. et al. An unfolded putative transmembrane polypeptide, which can lead to endoplasmic reticulum stress, is a substrate of Parkin. *Cell* **105**, 891–902 (2001).
15. Kitao, Y. et al. Pael receptor induces death of dopaminergic neurons in the substantia nigra via endoplasmic reticulum stress and dopamine toxicity, which is enhanced under condition of parkin inactivation. *Hum. Mol. Genet* **16**, 50–60 (2007).

16. Mattila, S. O., Tuusa, J. T. & Petäjä-Repo, U. E. The Parkinson's-disease-associated receptor GPR37 undergoes metalloproteinase-mediated N-terminal cleavage and ectodomain shedding. *J. Cell Sci.* **129**, 1366–1377 (2016).
17. Mattila, S. O. et al. GPR37 is processed in the N-terminal ectodomain by ADAM10 and furin. *FASEB J.* **35**, e21654 (2021).
18. Morató, X. et al. Ecto-GPR37: a potential biomarker for Parkinson's disease. *Transl. Neurodegener.* **10**, 8 (2021).
19. Marazziti, D. et al. GPR37 associates with the dopamine transporter to modulate dopamine uptake and behavioral responses to dopaminergic drugs. *Proc. Natl Acad. Sci. USA* **104**, 9846–9851 (2007).
20. Tousseyn, T. et al. ADAM10, the rate-limiting protease of regulated intramembrane proteolysis of Notch and other proteins, is processed by ADAMS-9, ADAMS-15, and the gamma-secretase. *J. Biol. Chem.* **284**, 11738–11747 (2009).
21. Braak, H., Alafuzoff, I., Arzberger, T., Kretzschmar, H. & Tredici, K. Staging of Alzheimer disease-associated neurofibrillary pathology using paraffin sections and immunocytochemistry. *Acta Neuropathol.* **112**, 389–404 (2006).
22. Koeglsperger, T. et al. Neuropathology of incidental Lewy body & prodromal Parkinson's disease. *Mol. Neurodegener.* **18**, 32 (2023).
23. Bang, S. et al. GPR37 regulates macrophage phagocytosis and resolution of inflammatory pain. *J. Clin. Invest* **128**, 3568–3582 (2018).
24. McCrary, M. R. et al. Protective effects of GPR37 via regulation of inflammation and multiple cell death pathways after ischemic stroke in mice. *FASEB J.* **33**, 10680–10691 (2019).
25. Marazziti, D. et al. Macroautophagy of the GPR37 orphan receptor and Parkinson disease-associated neurodegeneration. *Autophagy* **5**, 741–742 (2009).
26. Poewe, W. et al. Multiple system atrophy. *Nat Rev Dis Primers* **8**, 56 (2022).
27. Lane, C. A., Hardy, J. & Schott, J. M. Alzheimer's disease. *Eur. J. Neurol.* **25**, 59–70 (2018).
28. Xu, J. et al. Human striatal glia differentially contribute to AD- and PD-specific neurodegeneration. *Nat. Aging* **3**, 346–365 (2023).
29. Yuan, X. Z., Sun, S., Tan, C. C., Yu, J. T. & Tan, L. The Role of ADAM10 in Alzheimer's Disease. *J. Alzheimer's. Dis.* **58**, 303–322 (2017).
30. Oliveira Monteiro E Pereira de Almeida, M. P. et al. ADAM10 as a biomarker for Alzheimer's disease: A systematic review. *Rev. Neurol. (Paris)* https://doi.org/10.1016/j.neurol.2023.04.002 (2023).
31. Hayashida, K., Bartlett, A. H., Chen, Y. & Park, P. W. Molecular and cellular mechanisms of ectodomain shedding. *Anat. Rec.* **293**, 925–937 (2010).
32. Gandía, J. et al. The Parkinson's disease-associated GPR37 receptor-mediated cytotoxicity is controlled by its intracellular cysteine-rich domain. *J. Neurochem*. **125**, 362–372 (2013).
33. Lau, S. F., Cao, H., Fu, A. K. Y. & Ip, N. Y. Single-nucleus transcriptome analysis reveals dysregulation of angiogenic endothelial cells and neuroprotective glia in Alzheimer's disease. *Proc. Natl Acad. Sci. USA* **117**, 25800–25809 (2020).
34. Wolock, S. L., Lopez, R. & Klein, A. M. Scrublet: Computational Identification of Cell Doublets in Single-Cell Transcriptomic Data. *Cell Syst.* **8**, 281–291.e9 (2019).
35. Wolf, F. A., Angerer, P. & Theis, F. J. SCANPY: Large-scale single-cell gene expression data analysis. *Genome Biol*. **19**, 15 (2018).
36. Levine, J. H. et al. Data-Driven Phenotypic Dissection of AML Reveals Progenitor-like Cells that Correlate with Prognosis. *Cell* **162**, 184–197 (2015).
37. Lee, H. et al. Cell Type-Specific Transcriptomics Reveals that Mutant Huntingtin Leads to Mitochondrial RNA Release and Neuronal Innate Immune Activation. *Neuron* **107**, 891–908.e8 (2020).
38. Ravid, R. & Ferrer, I. Brain banks as key part of biochemical and molecular studies on cerebral cortex involvement in Parkinson's disease. *FEBS J.* **279**, 1167–1176 (2012).
39. Ferrer, I., Martinez, A., Boluda, S., Parchi, P. & Barrachina, M. Brain banks: Benefits, limitations and cautions concerning the use of post-mortem brain tissue for molecular studies. *Cell Tissue Bank* **9**, 181–194 (2008).
40. Braak, H. & Braak, E. Neuropathological stageing of Alzheimer-related changes. *Acta Neuropathol.* **82**, 239–259 (1991).
41. Braak, H. et al. Staging of brain pathology related to sporadic Parkinson's disease. *Neurobiol. Aging* **24**, 197–211 (2003).
42. Fahn, S., Elton, R. & Members of the UPDRS Development Committee. Unified Parkinson Disease Rating Scale. in *Recent Developments in Parkinson's Disease Vol II* (eds. Fahn, S., Marsden, C. D., Calne, D. B. & Goldstein, M.) (Macmillan Health Care Information, Florham Park, NJ, 1987).
43. Goetz, C. G. et al. Movement Disorder Society Task Force report on the Hoehn and Yahr staging scale: status and recommendations. *Mov. Disord.* **19**, 1020–1028 (2004).
44. Nasreddine, Z. S. et al. The Montreal Cognitive Assessment, MoCA: A Brief Screening Tool For Mild Cognitive Impairment. *J. Am. Geriatr. Soc.* **53**, 695–699 (2005).
45. Chaudhuri, K. R. et al. International multicenter pilot study of the first comprehensive self-completed nonmotor symptoms questionnaire for Parkinson's disease: the NMSQuest study. *Mov. Disord.* **21**, 916–923 (2006).
46. Zigmond, A. S. & Snaith, R. P. The hospital anxiety and depression scale. *Acta Psychiatr. Scand.* **67**, 361–370 (1983).
47. Tomlinson, C. L. et al. Systematic review of levodopa dose equivalency reporting in Parkinson's disease. *Mov. Disord.* **25**, 2649–2653 (2010).
48. Gilman, S. et al. Second consensus statement on the diagnosis of multiple system atrophy. *Neurology* **71**, 670–676 (2008).
49. Litvan, I. et al. Accuracy of clinical criteria for the diagnosis of progressive supranuclear palsy (Steele-Richardson-Olszewski syndrome). *Neurology* **46**, 922–930 (1996).
50. Armstrong, M. J. et al. Criteria for the diagnosis of corticobasal degeneration. *Neurology* **80**, 496–503 (2013).
51. Motulsky, H. J. & Brown, R. E. Detecting outliers when fitting data with nonlinear regression - A new method based on robust nonlinear regression and the false discovery rate. *BMC Bioinformatics* **7**, 123 (2006).

Acknowledgements

This work was supported by Ministerio de Ciencia, Innovación y Universidades-Agencia Estatal de Investigación-FEDER funds/European Regional Development Fund – "a way to build Europe" grants PID2020-118511RB-I00 to F.C., PID2022-141123OB-I00 to E.A., and Departament de Recerca i Universitats de la Generalitat de Catalunya (2021 SGR 00698). Founded by MCIN/AEI /10.13039/501100011033 "ESF Investing in your future" grant PRE2018-084480 to J.A., FPU19/03142 to L.G.-A., and PRE2021-098528 to P.A.-M. Also founded by PID2022-1365260B-I00 by MCIN/10.13039/501100011033 and ERD/EU and RyC programme RYC-2017-22594 to A.B.M.-M. We thank Centres de Recerca de Catalunya (CERCA) Programme/Generalitat de Catalunya for IDIBELL institutional support and Maria de Maeztu MDM-2017-0729 to Institut de Neurociencies, Universitat de Barcelona. We thank the Biology-Bellvitge Unit from Scientific and Technological Centers (CCiTUB), Universitat de Barcelona, and staff Esther Castaño and Benjamín Torrejón for their support and advice.

Author contributions

J.A., L.G., F.C. performed the data analysis. F.C. and J.A. wrote the manuscript. A.B.M.-M. provided resources, P.A.-B., P.S. provided materials for this manuscript including tissue samples and clinical data. J.A., M.L.-C., P.A.-M., L.G.-A. performed the experiments. S.B., A.G., K.A. provided pathology review and edited the manuscript. V.F.-D., A.M.-M., E.A. reviewed the manuscript and provided edits. P.S., F.C. conceived the manuscript and provided co-supervision for the project.

Competing interests
The authors declare no competing interests.

Additional information
Supplementary information The online version contains supplementary material available at https://doi.org/10.1038/s41531-024-00788-x.

Correspondence and requests for materials should be addressed to Per Svenningsson or Francisco Ciruela.

Reprints and permissions information is available at http://www.nature.com/reprints

Publisher's note Springer Nature remains neutral with regard to jurisdictional claims in published maps and institutional affiliations.

Open Access This article is licensed under a Creative Commons Attribution-NonCommercial-NoDerivatives 4.0 International License, which permits any non-commercial use, sharing, distribution and reproduction in any medium or format, as long as you give appropriate credit to the original author(s) and the source, provide a link to the Creative Commons licence, and indicate if you modified the licensed material. You do not have permission under this licence to share adapted material derived from this article or parts of it. The images or other third party material in this article are included in the article's Creative Commons licence, unless indicated otherwise in a credit line to the material. If material is not included in the article's Creative Commons licence and your intended use is not permitted by statutory regulation or exceeds the permitted use, you will need to obtain permission directly from the copyright holder. To view a copy of this licence, visit http://creativecommons.org/licenses/by-nc-nd/4.0/.

© The Author(s) 2024